Structure of White Dwarf Stars

JOSEPH ALLEN

University of Southampton, SO17 1BJ, United Kingdom

ja7g19@soton.ac.uk

Student ID: 31500145

This article investigates the structure of white dwarf stars, which are compact objects that represent the end-point of stellar evolution for low to intermediate-mass stars. The system was modelled on python as a relativistic free fermi gas, utilising a RK45 approach to determine the equation of state (mass-radius relationship). C/O/He and Fe white dwarf compositions were plotted from observational data (SDSS and PHYS6017) and found to be consistent within the non-relativistic, relativistic, and extremely relativistic regimes. The Chandrasekhar mass obtained for the C/O/He and Fe white dwarf stars are $1.44\ M_\odot$ and $1.22\ M_\odot$ respectively. This project was compiled on a HP Laptop 15s-eq1521sa, AMD 3020e.

1. INTRODUCTION

All stars under a critical value of $8\ M_\odot$ will end their lifespan as a white dwarf [1], these are a type of celestial object that have exhausted their nuclear fuel as a main sequence star in which the outer layers are ejected to form planetary nebulae leaving only the core behind. As fusion has ceased, the core no longer has any outward force to balance its own inward gravitational force, yet the core doesn't collapse in on itself due to their composition of electron-degenerate matter, which is the result of the pressure from the degenerate electrons in the core unable to occupy the same energy state and violate Pauli's exclusion principle [2]. As temperature falls to $T = 0K$, electrons begin to occupy lower energy levels until at the ground state upwards to the fermi level the fermion gas is said to be completely degenerate, a further explanation of this pressure comes in from of an analogy of Heisenberg's principle:

$$\Delta(x)\Delta(p) \geq \hbar/2$$

As the electron is confined to a smaller space, the momentum of the electron increases giving this pressure [3]. There is a limit to this degeneracy pressure as Chandrasekhar showed in the 1930s that if the star is modelled in hydrostatic equilibrium as a degenerate relativistic gas, the limit is $1.44\ M_\odot$. If this is exceeded, then the core collapses further to a neutron star or a black hole [4]. All white dwarfs below the critical limit will ultimately end their lives by cooling down gradually over billions of years, until they become 'black dwarfs'- cold, dark, and inert objects that emit no more heat or light. At this point in time, no such black dwarfs have been observed as the universe isn't old enough [5]. Alternatively, in a binary system a white dwarf can accrete matter from its companion till the critical limit is surpassed, leading to a type 1a supernova. In the following sections I will detail my methodology and interpretations of the data obtained.

2. METHODOLOGY

This article concerns the non-dimensionalisation of the of the differential equations relating pressure, density, mass, and radius. These are redefined with dimensionless variables to avoid errors from expressions dealing with both large numbers such as the speed of light and the miniscule mass of a proton. A substitution of these variables gives two first order ODES which are then integrated using a 4th order Runge-Kutta method to find the equation of state governing said white dwarves. The following assumptions are used in determining the validity of the known masses and radii of white dwarves: We assume the star is spherically symmetric and not rotating. The system is a relativistic free fermi gas and in hydrostatic equilibrium.

A. Substitution and Manipulation of Differential Equations

We consider a small cube of matter at a distance r from the centre with height δh and area δA. The gravitational force acting on it will be: (1)

$$F = \frac{-Gm(r)}{r^2}\delta h \delta A$$

Where G is the gravitational constant, $\rho(r)$ is the density at radius r, and m(r) is the mass contained within radius r. This force must equal the difference in pressure δP times δA, so that we have, (2)

$$\frac{dP}{dr} = \frac{-Gm(r)}{r^2}\rho(r)$$

Using the chain rule we can write: (3)

$$\frac{d\rho}{dr}\frac{dP}{d\rho} = \frac{-Gm(r)}{r^2}\rho(r)$$

Mass is fundamental in describing the structure of stars and so it is important to know how it changes within a given star. Density is given as mass per unit volume which leads to our first main equation: (4)

$$\frac{dm}{dr} = 4\pi r^2 \rho(r)$$

As derived in the appendix, our second main equation relates density and radius with pressure and mass. (5)

$$\frac{d\rho}{dr} = -\frac{d\rho}{dP}\frac{Gm(r)}{r^2}\rho(r)$$

Note that $\frac{dP}{d\rho}$ varies on whether we model the star as a non-relativistic or an extremely relativistic fermi gas. (6)

$$\frac{dP}{d\rho} = Y_e\frac{m_e c^2}{m_p}\gamma(\frac{\rho}{\rho_0})$$

This is known as the equation of state for a white dwarf modelled as a relativistic free fermi gas, where Y_e is the number of electrons per nucleon, γ is the gamma function: (7)

$$\gamma(y) = \frac{y^{\frac{2}{3}}}{3\sqrt{(1+y^{\frac{2}{3}})}}$$

We introduce the variables x,y and z to redimensionalise radius, mass and density respectively. (8)(9)(10) x=$\frac{r}{R_0}$ y=$\frac{m}{M_0}$ z=$\frac{\rho}{\rho_0}$ R_0 is chosen such that all dimensionless constants are absorbed in equations, ρ_0 is the natural unit for density and $\frac{4\pi\rho_0 R_0^3}{3}$ is a natural unit for mass. These dimensionless quantities vary only between 1 and 0 such to avoid errors caused by computing with large numbers and small numbers. Equations (9) and (10) are substituted into (4); (8), (9) and (10) are substituted into (5) to give the following dimensionless equations.

$$\frac{dy}{dx} = 3x^2 z$$

$$\frac{dz}{dx} = \frac{-Ayz}{x^2\gamma(z)}$$

Where constant $A = \frac{4\pi G R_0^2 \rho_0 m_p}{3Y_e m_e c^2}$

B. How is Runge-Kutta implemented?

All computational analysis was done on Spyder (Python) using RK45 within the solve ivp function. To produce the density profile a boundary condition: $\frac{\rho}{\rho_0} = 0$ when $x = 0$ is placed so that density is positive for a star with physical volume. Values of $Y_e = 0.5$ and $Y_e = 0.46$ are chosen for the carbon and iron core white dwarves, so that that the dimensionless differential equations can be integrated over these Y_e values. The number of iterations is chosen to balance the precision of the answer and the length of time to run the algorithm. Referring to last semester's numerical methods module, the error in the values produced due to truncation are dealt with by comparing the value received for each order of Runge-Kutta method. Further boundary conditions are $x = 0$, $y = 0$ and $z = 1$ and while the value of the density is greater than $\frac{1}{M_0(0.5)}$, the program continues to run. This is chosen such that we avoid a zero-division error. The values of x and z are thus given dimension by converting back into solar units and plotted against each other, so a density profile is obtained. To produce a plot of mass against radius (equation of state), a range of central densities (ρ_c) 10^6 to 10^{15} were chosen to be looped over each value of Y_e for each of the dimensionless differential equations. With each iteration of ρ_c, the final value of mass and radius is converted to solar units and then appended to an array once the boundary condition $\rho = \rho_c$ is achieved. As part of the guidance offered by PHYS6017, data concerning the mass and radius of three white dwarves (including error bars) are plotted along with the variation of mass and radii to validate these values and thus show the necessity for the initial assumptions in completing this article.

3. RELATIVISTIC CASE

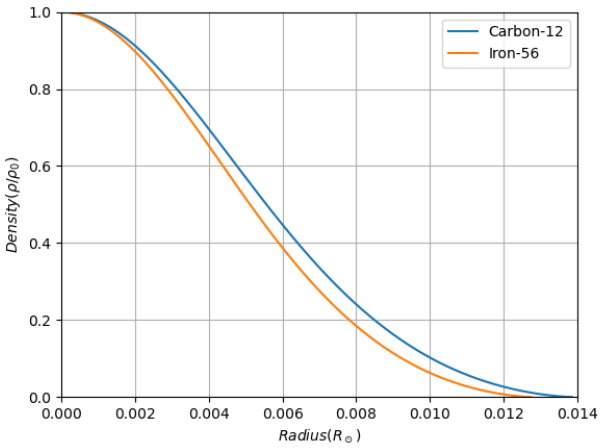

Fig. 1. Density profile for a C^{12} and Fe^{56} core white dwarves.

Dimensionless quantities z and x are plotted against each other to assess the variation of density as the radial distance increases. The core composition makes a difference for the entirety of the graph as the Fe^{56} white dwarves are less dense than the C^{12} cores leading to maximum radii values of 0.0139 $R_\odot$ for C^{12} cores and 0.0127 $R_\odot$ for Fe^{56} cores. The relationship follows a linear relationship for the middle portion then adopts a power law when nearing the maximal radii. Iron cores became less dense than the carbon counterpart faster with increased radial distance from the centre, suggesting that more mass is enclosed within a smaller radius with possible envelopes of elements sharing similar Y_e. In normal stars this would result in a higher temperature however in this article we consider the system as degenerate, temperature has no effect on any of the other physical properties of the star.

A plot of solar mass against solar radius has shown that Procyon B falls within the limits of the C^{12} core model whilst Stein 2051 and 40 Eri B fall within the Fe^{56} core model. White dwarfs typically fuse up to carbon, yet Iron cores can arise from high mass stars fusing up to Iron in their cores which have their outer envelopes ripped away by accretion from a binary star. Typically, we would associate a larger mass star as having a larger radius, however as shown in figure 2, a slight increase in mass causes a dramatic drop in solar radius. The curve can be described as an ideal gas pressure with a high-power law representing the fast drop-off. The increase in gravitational force on the white dwarf in this instance can be seen as the independent variable, whilst the electron degeneracy is kept relatively constant. The drop in solar radius continues until we reach the Chandrasekhar limit, M_{Ch}, where the electron degeneracy pressure is overcome and the core collapses further to a neutron star or a black hole. In some instances, the white dwarf is part of a binary system and can accrete mass from its partner star and trigger a type 1a supernova. This event would have a luminosity exceeding $10^{43}\frac{erg}{sec}$, billions of times that of our sun [6]. During the middle portion

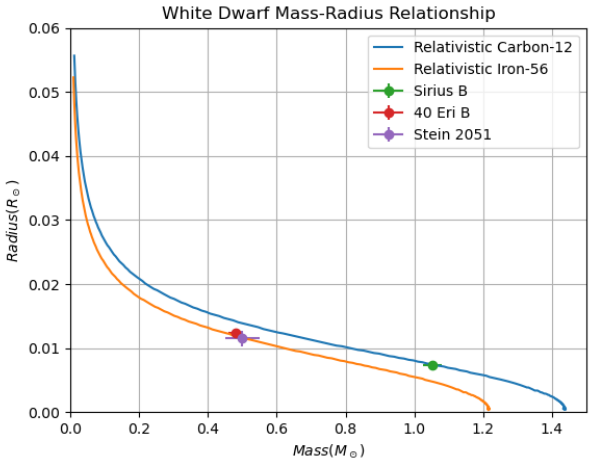

Fig. 2. The equation of state for C^{12} and Fe^{56} white dwarves modelled as a relativistic free fermi gas.

of the graph the slope levels out as we enter the near-relativistic regime which has an equation of state of gradient equal to $-\frac{1}{3}$, P can be approximated to $\rho^{\frac{5}{3}}$, and a polytropic index of $\frac{3}{2}$. As we enter the extremely relativistic regime, the radius decreases quickly to our Chandrasekhar mass M_{Ch}, giving a mass limit of 1.44 $M_\odot$ for the C^{12} cores and 1.22 $M_\odot$ for the Fe^{56} cores which agrees with theory available online (1.4 to 1.44 $M_\odot$).[7].

Table 1. White Dwarf parameters

Parameter:	Mass $M_\odot$	Radius $R_\odot$
Sirius B	1.053 ± 0.028	0.0074 ± 0.0006
40 Eri B	0.48 ± 0.02	0.0124 ± 0.0005
Stein 2051	0.50 ± 0.05	0.0115 ± 0.0012

Where the solar units are equals to $M_\odot = 1.98 \times 10^{30} kg$ and $R_\odot = 6.95 \times 10^{8} m$

4. NON-RELATIVISTIC AND EXTREMELY RELATIVISTIC CASE

Table 2. SDSS Dataset Release

Parameter:	Mass $M_\odot$	Radius $R_\odot$
SDSS J0024+1745	0.534 ± 0.009	0.0140 ± 0.0007
SDSS J1028+0931	0.415 ± 0.004	0.0177 ± 0.0002
SDSS J1307+2156	0.436 ± 0.002	0.0157 ± 0.0004

Where the solar units are equals to $M_\odot = 1.98 \times 10^{30} kg$ and $R_\odot = 6.95 \times 10^{8} m$

As an extension for this article, three white dwarf data points found in the SDSS Data Release are plotted (black) alongside the WD data given by PHYS6017 discussed previously. Considering the appropriate error bars, they fall within the constraints of the model. However, it is important to note that the study in which these points are taken from state that envelopes of other elements with identical Y_e values may be present within the WD core, therefore it is crucial that these are not treated as solely C^{12} or Fe^{56} white dwarves.

As a further extension, non-relativistic and extremely relativistic regimes are plotted using methods detailed within the appendix. As seen in figure 3, the extremely relativistic case, $v(p) = c$ represents the limit at the numerical Chandrasekhar mass and is a straight line. The non-relativistic case is identical to the relativistic case in the low mass regime yet deviates from the relativistic case at around 0.18 $M_\odot$ and extends past the Chandrasekhar masses as it slowly tends to zero. Non-relativistic white dwarves will gradually radiate away their energy, causing it to cool down and dim. Eventually, it will stop emitting a noticeable amount of visible light and transform into a black dwarf. The cooling process of a white dwarf to reach the black dwarf stage is estimated to take about 10^{15} years, which is longer than the current age of the universe[9].

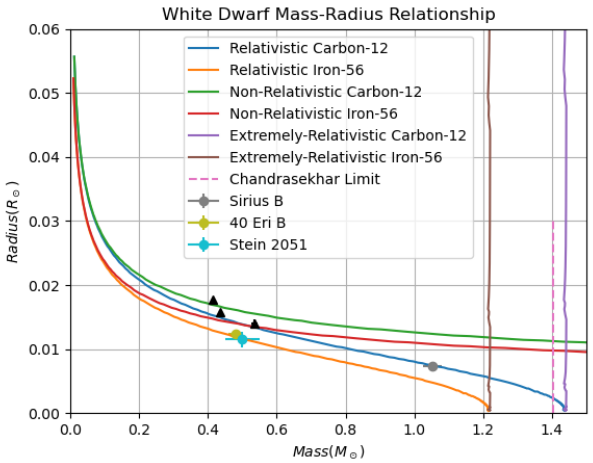

Fig. 3. Addtional data on white dwarves taken from the SDSS datset overlayed [8]. The theoretical Chandrasekhar limit is plotted as well as the non-relativistic and extremely relativistic regimes.

5. LIMITATIONS OF THIS ARTICLE

The following limitations of this article are an obstacle in validating the assumptions for this model: The lack of first-hand data for the mass and radius of white dwarves coupled with the quantitative lack of observed data points in other studies. More comparisons are needed to make this model more conclusive. Incorrect assumptions are made that C/O/He core WDs are identical based on their Y_e values and that the outer envelopes can be disregarded. To properly describe the mass-radius relationship, it is necessary to differentiate between elements of the same Y_e and consider the impact of thin envelopes of hydrogen and helium spoiling the physics of the model. To counteract this, a density function considering these envelopes should be implemented to monitor the fluctuating densities over the radius of the star.

White dwarves have an extremely long thermal timescale. Since there is no fusion process taking place, they gradually emit their energy and cool over time, ultimately becoming a black dwarf. Despite their theoretical existence, black dwarfs

have not been directly observed because of the extended thermal timescale involved. Nevertheless, it would be worthwhile to explore the impact of cooling on white dwarves through further research. It should also be noted that the magnetic fields of these WDs have been overlooked in this article, which inevitably affects their mass and radius.

Surpassing the Chandrasekhar limit could offer an extension to this article. Beyond the Chandrasekhar limit a white dwarf can end its lifecycle along three paths which all depend on the balance between electron/neutron degeneracy pressure and the pressure due to gravity [10]. Firstly, the accretion from a red giant or main sequence star leading to a type 1a supernova as discussed previously. Secondly, a collision between two white dwarves could disrupt the pressure balance, causing the less massive one to be accreted by the more massive white dwarf. The latter then collapses before thermonuclear runaway. Thirdly, helium in the outer envelope of a C/O white dwarf may suddenly undergo fusion to C/O leading to the gravitational pressure being greater than the degeneracy pressure, causing the core to ignite.

The observed mass-radius relationship of white dwarves may be influenced by their rotation. This phenomenon, which is currently a topic of research, is not yet entirely comprehended but is thought to be responsible for deviations in luminosity and masses exceeding the Chandrasekhar limit. To examine the changes in the mass-radius relationship, it is possible to investigate either rigid rotation, which leads to lower masses, or differential rotation, which leads to higher masses. Additionally, some WDs are known to pulsate, causing further alterations to the mass-radius relationship [11].

6. CONCLUDING STATEMENTS

This article investigates the structure of white dwarf stars, which are compact objects that represent the endpoint of stellar evolution for low to intermediate-mass stars. The system was modelled on python as a relativistic free fermi gas, utilising a RK45 approach to determine the equation of state (mass-radius relationship). C/O/He and Fe white dwarf compositions were plotted from observational data (SDSS and PHYS6017) and found to be consistent within the non-relativistic, relativistic, and extremely relativistic regimes. The density-radius graphs for both a single white dwarf and all WDs plotted against mass and radius support the theory introduced earlier. By introducing some assumptions, a simplified method was born. The Chandrasekhar mass for white dwarves with C/O/He and Fe cores were calculated, producing values of 1.44 $M_\odot$ and 1.22 $M_\odot$, respectively, which agree with previously recorded results. Based on the tested regimes, it can be concluded that the relativistic model is the appropriate model.

7. APPENDIX

For a relativistic gas,

$$Pressure(P) = \frac{\int_0^\infty n(p) p v(p) dp}{3}$$

Where $n(p)$ is,

$$\frac{8\pi p^2}{h^3}$$

$$if p < p_{fermi}$$

p_{fermi} is given by,

$$p_{fermi} = \sqrt[3]{\frac{3h^3 p}{8\pi\mu m_u}}$$

This is followed from a rearrangement of,

$$n = \int_0^{p_{fermi}} \frac{8\pi p^2}{h^3} dp = \frac{8\pi p_{fermi}^3}{3h^3}$$

The energy of a relativstic gas is given by,

$$p^2c^2 + m_e^2c^4 = \gamma^2 m_e^2 c^4$$

Which leads us to give $v(p)$ as,

$$v(p) = c\sqrt{1 - \frac{1}{1 + (\frac{p}{m_e c^2})^2}}$$

Substitution of this into our expression for pressure gives,

$$Pressure(P) = \int_0^{p_{fermi}} \frac{8\pi p^3 v(p_{fermi})}{3h^3} dp$$

As mentioned in the methodology, we use the chain rule: $\frac{dP}{d\rho} = \frac{dP}{dp}\frac{dp}{d\rho}$

$$\frac{dP}{d\rho} = \frac{8\pi p_{fermi}^3 v(p_{fermi})}{3h^3} \frac{dp}{d\rho}(p_{fermi})$$

Substituting the expression for the fermi momentum gives,

$$\frac{dP}{d\rho} = \frac{c\sqrt[3]{\rho}}{3\mu m_u} \sqrt{\frac{1}{1 + (\frac{m_e c^2}{p_{fermi}})}} \sqrt[3]{\frac{3h^3}{8\pi\mu m_u}}$$

Using the dimesionless variable $z = \frac{\rho}{\rho_0}$ and approximating the fermi momentum as $\sqrt[3]{p}$ we can conclude that,

$$\frac{dP}{d\rho} = \frac{Y_e m_e c^2 y^{\frac{2}{3}}}{3m_p\sqrt{(1 + y^{\frac{2}{3}})}}$$

For a non-relativistic gas we revert back to the classical formula for velocity, $v(p) = \frac{p}{m_e}$ which alters the pressure P as:

$$Pressure(P) = \int_0^{p_{fermi}} \frac{n(p) p^2}{3m_e} dp$$

Using the methods above, for the non-relativistic case we arrive at,

$$\frac{dP}{d\rho} = \frac{Y_e m_e c^2}{3m_p} \sqrt[3]{(\frac{\rho}{\rho_0})^2}$$

By defining similar dimensionless variables, similar to that of the relativistic case we have the dimensionless equations to be integrated via RK45. (Note that $\frac{dy}{dx}$ remains the same as the relativistic case)

$$\frac{dz}{dx} = -B\frac{z^{\frac{1}{3}} y}{x^2}$$

Where the constant B=$\frac{4\pi G R_0^2 \rho_0 m_p}{Y_e m_e c^2}$ In the extremely relativistic case, velocity tends to the speed of light giving a different expression for gas pressure,

$$Pressure(P) = \int_0^{p_{fermi}} \frac{n(p) p c}{3} dp$$

As above by following the methods above we arrive at,

$$\frac{dP}{d\rho} = \frac{Y_e m_e c^2}{3m_p} \sqrt[3]{\frac{\rho}{\rho_0}}$$

Dimensionless equations to be integrated via RK45 (Note that $\frac{dy}{dx}$ remains the same as the non-relativistic case) are:

$$\frac{dz}{dx} = -B\frac{z^{\frac{2}{3}}y}{x^2}$$

8. RUNGE-KUTTA METHODS IN ACADEMIA AND INDUSTRY

In industry Runge-Kutta have the following uses:

Within aerospace Runge-Kutta methods are employed in designing and analyzing aircraft and missile systems [12]. These methods help simulate the movement of the aircraft in diverse flight conditions and optimize the design parameters. These also are also helpful in predicting the behavior of rockets and missiles during flight and launch and in determining the effect of various factors such as wind and atmospheric conditions.

In chemical engineering, Runge-Kutta methods are used to simulate and model chemical processes in the chemical industry. These methods simulate chemical reactors' behavior, including reactions involving multiple phases, and optimize operating conditions to achieve desired product yields and purity [13]. Additionally, these are also used in designing chemical process control systems, including temperature, pressure, and flow rate control.

In terms of the automotive industry, Runge-Kutta methods are utilized in the design and analysis of automotive systems, such as engine and transmission control systems [14]. These methods simulate the behavior of engine and transmission systems, including the interaction of multiple components, and optimize control parameters for improved performance and fuel efficiency.

In academia Runge-Kutta have the following uses:

Within partial differential equations, Runge-Kutta methods are widely used to solve partial differential equations that arise in several fields, including fluid dynamics, electromagnetism, and quantum mechanics [15]. These methods are often combined with finite element or finite difference methods to approximate the solution of PDEs accurately.

For machine learning, Runge-Kutta methods are sometimes used in machine learning applications to solve optimization problems that arise in this field. For instance, researchers have used these methods to optimize the weights of neural networks and to solve reinforcement learning problems [16].

In terms of signal processing, Runge-Kutta methods are also used in signal processing applications, such as digital filtering and image processing. These methods help approximate the solution of differential equations that arise in signal processing problems [17]. For example, researchers have used Runge-Kutta to develop digital filters that can remove noise from signals and improve image quality.

9. REFERENCES

1. 1982AA...108..406K Page 406 [Internet]. [cited 2023 Apr 14]. Available from: https://adsabs.harvard.edu/full/1982A

2. Barstow MA, Werner K. Structure and evolution of white dwarfs and their interaction with the local interstellar medium. In: Gómez de Castro AI, Wamsteker W, editors. Fundamental Questions in Astrophysics: Guidelines for Future UV Observatories [Internet]. Dordrecht: Springer Netherlands; 2006 [cited 2023 Apr 14]. p. 3–16. Available from: https://doi.org/10.1007/978-1-4020-4839-5_1

3. White dwarfs and electron degeneracy [Internet]. [cited 2023 Apr 14]. Available from: http://hyperphysics.phy-astr.gsu.edu/hbase/Astro/whdwar.html

4. Pal SK, Nandi P. Effect of dynamical noncommutativity on the limiting mass of white dwarfs. Physics Letters B [Internet]. 2019 Oct 10 [cited 2023 Apr 14];797:134859. Available from: https://www.sciencedirect.com/science/article/pii/S0370269319305738

5. Gaensler BM, Slane PO. The evolution and structure of pulsar wind nebulae. Annu Rev Astron Astrophys [Internet]. 2006 Sep 1 [cited 2023 Apr 14];44(1):17–47. Available from: https://www.annualreviews.org/doi/10.1146/annurev.astro.44.051905.092

6. Type ia supernovae - an overview | sciencedirect topics [Internet]. [cited 2023 Apr 14]. Available from: https://www.sciencedirect.com/topics/physics-and-astronomy/type-ia-supernovae: :text=A

7. Chandrasekhar limit | astronomy | Britannica [Internet]. [cited 2023 Apr 14]. Available from: https://www.britannica.com/science/Chandrasekhar-limit

8. Parsons SG, Gänsicke BT, Marsh TR, Ashley RP, Bours MCP, Breedt E, et al. Testing the white dwarf mass-radius relationship with eclipsing binaries. Monthly Notices of the Royal Astronomical Society [Internet]. 2017 Oct [cited 2023 Apr 14];470(4):4473–92. Available from: http://arxiv.org/abs/1706.05016

9. Panei JA, Althaus LG, Chen X, Han Z. Full evolution of low-mass white dwarfs with helium and oxygen cores. Monthly Notices of the Royal Astronomical Society [Internet]. 2007 Dec 1 [cited 2023 Apr 14];382(2):779–92. Available from: https://academic.oup.com/mnras/article-lookup/doi/10.1111/j.1365-2966.2007.12400.x

10. Dan M, Rosswog S, Guillochon J, Ramirez-Ruiz E. How the merger of two white dwarfs depends on their mass ratio: orbital stability and detonations at contact. Monthly Notices of the Royal Astronomical Society [Internet]. 2012 May 21 [cited 2023 Apr 14];422(3):2417–28. Available from: http://arxiv.org/abs/1201.2406

11. Hachisu I, Kato M, Nomoto K. Final fates of rotating white dwarfs and their companions in the single degenerate model of type ia supernovae. ApJL [Internet]. 2012 Aug 8 [cited 2023 Apr 14];756(1):L4. Available from: https://iopscience.iop.org/article/10.1088/2041-8205/756/1/L4/meta

12. Persson PO. High-order les simulations using implicit-explicit runge-kutta schemes. In: 49th AIAA Aerospace Sciences Meeting including the New Horizons Forum and Aerospace Exposition [Internet]. Orlando, Florida: American Institute of Aeronautics and Astronautics; 2011 [cited 2023 Apr 14]. Available from: https://arc.aiaa.org/doi/10.2514/6.2011-684

13. Kaps P, Rentrop P. Application of a variable-order semi-implicit Runge-Kutta method to chemical models. Computers Chemical Engineering [Internet]. 1984 Jan 1 [cited 2023 Apr 14];8(6):393–6. Available from: https://www.sciencedirect.com/science/article/pii/0098135484900097

14. Kennedy CA, Carpenter MH, Lewis RM. Low-storage, explicit Runge–Kutta schemes for the compressible Navier–Stokes equations. Applied Numerical Mathematics [Internet]. 2000 Nov 1 [cited 2023 Apr 14];35(3):177–219. Available from: https://www.sciencedirect.com/science/article/pii/S0168927499001415

15. van der Houwen PJ. The development of Runge-Kutta methods for partial differential equations. Ap-

plied Numerical Mathematics [Internet]. 1996 Mar 1 [cited 2023 Apr 14];20(3):261–72. Available from: https://www.sciencedirect.com/science/article/pii/0168927495001093

16. Stillfjord T, Williamson M. SRKCD: A stabilized Runge–Kutta method for stochastic optimization. Journal of Computational and Applied Mathematics [Internet]. 2023 Jan 1 [cited 2023 Apr 14];417:114575. Available from: https://www.sciencedirect.com/science/article/pii/S0377042722002837

17. Söderlind G. Time-step selection algorithms: Adaptivity, control, and signal processing. Applied Numerical Mathematics [Internet]. 2006 Mar 1 [cited 2023 Apr 14];56(3):488–502. Available from: https://www.sciencedirect.com/science/article/pii/S0168927405000954